

Clouds as turbulent density fluctuations. Implications for pressure confinement and spectral line data interpretation

Javier Ballesteros-Paredes¹, Enrique Vázquez-Semadeni¹, and John Scalo²

¹*Instituto de Astronomía, Universidad Nacional Autónoma de México
Apdo. Postal 70-264, 04510 México D.F., México. e-mail: javier,enro@astroscu.unam.mx*

²*Astronomy Department, University of Texas, Austin, TX 78712-1083.
e-mail: parrot@astro.as.utexas.edu*

ABSTRACT

We examine the idea that diffuse and giant molecular clouds and their substructure form as density fluctuations induced by large scale interstellar turbulence. We do this by closely investigating the topology of the velocity, density and magnetic fields within and at the boundaries of the clouds emerging in high-resolution two-dimensional simulations of the ISM including self-gravity, magnetic fields, parameterized heating and cooling and a simple model for star formation. We find that the velocity field is continuous across cloud boundaries for a hierarchy of clouds of progressively smaller sizes. Cloud boundaries defined by a density-threshold criterion are found to be quite arbitrary, with no correspondence to any actual physical boundary, such as a density discontinuity. Abrupt velocity jumps are coincident with the density maxima, indicating that the clouds are formed by colliding gas streams. This conclusion is also supported by the fact that the volume and surface kinetic terms in the Eulerian Virial Theorem for a cloud ensemble are comparable in general. The topology of the magnetic field is also suggestive of the same process, exhibiting bends and reversals where the gas streams collide. However, no unique trend of alignment between density and magnetic features is observed. Both sub- and super-Alfvénic motions are observed within the clouds in the simulations.

In the light of these results, we argue that thermal pressure equilibrium is irrelevant for cloud confinement in a turbulent medium, since inertial motions can still distort or disrupt a cloud, unless it is strongly gravitationally bound. Turbulent pressure confinement appears self-defeating, because turbulence contains large-scale motions which necessarily distort Lagrangian cloud boundaries, or equivalently cause flux through Eulerian boundaries.

We then discuss the compatibility of the present scenario with observational data. We find that density-weighted velocity histograms are consistent with observational line profiles of comparable spatial and velocity resolution, exhibiting similar FWHMs and similar multi-component structure. An analysis of the regions contributing to each velocity interval indicates that the histogram “features” do not come from isolated “clumps”, but rather from extended regions throughout a cloud, which often have very different total velocity vectors.

Finally, we argue that the scenario presented here may be also applicable to small scales with larger densities (molecular clouds and their substructure, up to at least $n \sim 10^3\text{--}10^5 \text{ cm}^{-3}$), and conjecture that quasi-hydrostatic configurations cannot be produced from turbulent fluctuations unless the thermodynamic behavior of the flow becomes nearly adiabatic. We demonstrate, using appropriate cooling rates, that this will not occur except for very small compressions ($\lesssim 10^{-2}$ pc) or until protostellar densities are reached for collapse.

1. Introduction

Theoretical models of interstellar clouds and clumps most frequently assume static or stationary configurations, the clouds being either confined by the external pressure (Maloney 1988; Bertoldi & McKee 1992, hereafter BM92), or in “virial equilibrium” between its self-gravity and some form of internal energy, be it thermal (e.g., Chièze 1987), micro-turbulent (e.g., Chandrasekhar 1951; Bonazzola et al. 1987; Léorat, Passot & Pouquet 1990; Vázquez-Semadeni & Gazol 1995) or magnetic (e.g., Shu, Adams & Lizano 1987; Mouschovias 1987, Myers & Goodman, 1988b), forming out of instabilities or coagulation of smaller clouds (see Elmegreen 1993a for a review). Nevertheless, the interstellar medium (ISM) is well known to be highly violent (e.g., McCray & Snow 1979), and recently it has become increasingly accepted that it is turbulent throughout (e.g., Scalo 1987; see also the volume “Interstellar Turbulence” [Franco & Carramiñana 1998]). In such a medium, clouds may naturally form as turbulent density fluctuations as well.

Within this dynamic, turbulent framework, it is important to reconsider the meaning and feasibility of pressure cloud confinement, either thermal or turbulent. This is most adequately done in the context of the Virial Theorem (VT), which is a very useful tool for describing the balance between all the physical agents in molecular clouds. Customarily, the VT is considered in a Lagrangian frame, i.e., a frame moving with the flow. However, there are circumstances when one would prefer to use an Eulerian description. For example, a Lagrangian description is clearly not well suited for describing the propagation of a wave, in which the fluid does not move along with the perturbation, while in the case of an isolated object a Lagrangian description fits most naturally (see also Vázquez-Semadeni, Passot & Pouquet 1996, hereafter VSP96). In the interstellar case, if significant mass exchange occurs between a cloud and its surroundings, such as an accreting cloud, an Eulerian (fixed in space) may be preferable since a Lagrangian boundary would undergo severe distortions. Parker (1969) derived an Eulerian form of the Virial Theorem (EVT) in tensor form, but he explicitly neglected the mass flux through the surface of the cloud. More recently, McKee & Zweibel (1992) (hereafter MZ92) have written all the terms entering the EVT:

$$\frac{1}{2}\ddot{I}_E = 2\left(\mathcal{E}_{\text{th}} + \mathcal{E}_{\text{kin}} - \mathcal{T}_{\text{th}} - \mathcal{T}_{\text{kin}}\right) + \mathcal{M} + \mathcal{W} - \frac{1}{2}\frac{d\Phi}{dt}, \quad (1)$$

where $I_E \equiv \int_V \rho r^2 dV$ is the moment of inertia of the cloud, $\mathcal{E}_{\text{th}} \equiv 3/2 \int_V P_{\text{th}} dV$ is the thermal energy, with P_{th} being the thermal pressure; $\mathcal{E}_{\text{kin}} \equiv 1/2 \int_V \rho u^2 dV$ is the kinetic energy, $\mathcal{T}_{\text{th}} \equiv 1/2 \oint_S x_i P_{\text{th}} \hat{n}_i dS$ is the surface thermal term, $\mathcal{T}_{\text{kin}} \equiv 1/2 \oint_S x_i \rho u_i u_j \hat{n}_j dS$ is the surface kinetic term, $\mathcal{M} \equiv 1/8\pi \int_V B^2 dV + \int_S x_i T_{ij} \hat{n}_j dS$ is the magnetic term, with T_{ij} the Maxwell stress tensor, $\mathcal{W} \equiv \int_V \rho x_i g_i dV$ is the gravitational term and $\Phi \equiv \oint_S \rho x^2 u_i \hat{n}_i dS$ is the flux of moment of inertia through the surface of the cloud. Sums over repeated indices are assumed unless otherwise stated.

Frequently, the surface terms are neglected altogether, especially in observational work (Larson 1981; Torrelles et al, 1983; Myers & Goodman, 1988a; Fuller & Myers 1992), although it is also a common practice in theoretical studies, as a consequence of assuming isolated clouds (e.g., Chandrasekhar & Fermi 1953; Parker 1969, Parker 1979). The most notable exception is the thermal pressure surface term \mathcal{T}_{th} , which is frequently invoked for “pressure confinement” (e.g. McCrea 1957; Keto & Myers, 1986; Maloney 1988; BM92; McLaughlin & Pudritz 1996; Yonekura et al. 1997). By analogy, MZ92 have considered the possibility of turbulent pressure confinement by means of the term \mathcal{T}_{kin} . However, in the present paper we will argue that both kinds of pressure confinement require idealized conditions that are not likely to be realized in the actual ISM. If the interstellar medium (ISM) is globally turbulent, the velocity field is in general locally nonzero, and thermal pressure balance may be irrelevant, since a cloud can still undergo deformation due to the inertial motions, which will induce a nonzero RHS via the kinetic terms \mathcal{E}_{kin} , \mathcal{T}_{kin} , and $d\Phi/dt$.

Concerning turbulent pressure confinement, its feasibility requires the underlying assumption that the turbulence be microscopic, so that it can be considered isotropic compared to the scale of the cloud. However, turbulence is inherently a multi-scale phenomenon, and is expected to contain excitation at scales comparable or even larger to that of the cloud. It is in this context that the clouds may be considered as density fluctuations produced by larger-scale compressive turbulent motions (e.g., Hunter 1979; Lar-

son 1981; Hunter & Fleck 1982; Hunter et al. 1986; Elmegreen 1993b; Vázquez-Semadeni, Passot & Pouquet 1995, hereafter VSPP95). Such clouds are then turbulent fluctuations, and can either rebound, fragment or collapse depending on the compressive energy available, the cooling ability of the flow, the topology of the velocity and magnetic fields, the production of internal turbulent motions and a number of instability mechanisms (e.g., Elmegreen & Elmegreen 1978; Vishniac 1983, 1994; Hunter et al. 1986; Tohline, Bodenheimer & Christodoulou 1987; Stevens et al. 1992; Elmegreen 1993b; VSPP96; Kornreich & Scalo 1998).

Note that in this scenario, clouds and clumps need not be in a static or quasi-static equilibrium at any time. Moreover, the fact that clouds and clumps are observed to be internally turbulent suggests that the turbulence has not been completely dissipated inside. In fact, it is known that shocks running obliquely through a density gradient will produce further internal turbulence (Klein et al. 1995; Kornreich & Scalo 1998).

In this paper, we analyze the density, velocity and magnetic fields in two-dimensional numerical simulations of turbulence in the ISM in order to estimate the importance of the transport processes through the cloud boundaries. We start in §2 by discussing the role of the kinetic terms in the Virial Theorem and the implications for pressure confinement. Then, after briefly describing the numerical simulations (§3), we proceed to a description of our results (§4), starting with a discussion of the density, velocity and magnetic features that arise, and their spatial correlations (§4.1). Then we present an evaluation of the surface and volume kinetic terms in the virial theorem, suggesting that their similarity may be indicative that both types of terms are representative of the same phenomenon (§4.2). The super- or sub-Alfvénic character of the motions is discussed in §4.3. In §5 we present several comparisons with known observational data, such as line profiles observed in cloud complexes (§5.1), the topology of the magnetic field (§5.2), and the lifetimes of the clouds (§5.3). In §6 we then discuss several issues and possible caveats, like whether the scenario proposed here can be applicable to smaller, denser scales, the low probability of forming quasistatic clumps in a turbulent medium, and the effect of the dimensionality of our simulations. Finally, we give a summary and some conclusions in §7.

2. Kinetic Terms in the Eulerian Virial Theorem

As is well known (e.g., Parker 1969; MZ92), the EVT can be obtained from the conservative form of the momentum equation,

$$\frac{\partial(\rho u_i)}{\partial t} + \frac{\partial(\rho u_i u_j)}{\partial x_j} = \sum_k F_k \quad (2)$$

(where F_k generically represents the various force densities involved in the problem) by dotting it with the position vector \mathbf{x} and integrating over a volume V fixed in space. We remind the reader that the full Virial Theorem, eq. (1), holds always because it is a direct consequence of the momentum equation, although this does not necessarily imply that the system is in equilibrium or, in particular, that the linewidth of an interstellar cloud is directly related to its mass and radius (Maloney 1988). A detailed analysis of the VT in our simulations will be presented elsewhere (Ballesteros-Paredes et al. 1998).

In the present paper we focus on the relative importance of the surface and volumetric kinetic terms, and their role in shaping the clouds. It can be easily checked that, in the EVT (eq. [1]), the kinetic energy \mathcal{E}_{kin} , the kinetic surface term \mathcal{T}_{kin} , and the time-derivative terms \dot{I}_E and $d\Phi/dt$, originate from the LHS in the momentum equation (eq. [2]). While the meaning of the kinetic energy term \mathcal{E}_{kin} is obvious, the kinetic surface term \mathcal{T}_{kin} has two possible interpretations. One is as half the flux of the instantaneous rate of change of the moment of inertia $\rho x_i u_i$ through the cloud's surface. Alternatively, it can be interpreted as the sum of the ram pressure plus the kinetic stresses, both evaluated at the surface of the cloud:

$$\oint_S x_i \rho u_i u_j \hat{n}_j dS = \oint_S x_i \rho u^2 \hat{n}_i dS + \oint_S x_i \rho u_i u_j \hat{n}_j dS, \quad (3)$$

where $i \neq j$ in the last surface integral. The first term on the RHS of the eq. (3) is analogous to the thermal pressure surface term. The second term, on the other hand, reflects the fact that the turbulent motions are not isotropic, giving off-diagonal contributions to the total pressure tensor $\Pi_{ij} = P_{\text{th}} \delta_{ij} + \rho u_i u_j$ (Landau & Lifshitz 1987). This exhibits in a clear way the difference between the isotropic nature of the thermal

pressure and the anisotropic nature of the “turbulent” pressure.

Another important difference between the thermal and “turbulent” pressures lies in the fact that the latter is in general expected to involve motions of scales comparable to that of the cloud, as mentioned in §1. But since the velocity field carries mass with it, such large-scale motions necessarily imply a mass flux across fixed, Eulerian cloud boundaries. Conversely, in a Lagrangian description, such turbulent motions should lead to severe distortions of the Lagrangian cloud boundary, possibly giving it a fractal character (e.g., Scalo 1990; Falgarone, Phillips & Walker 1991).

The exception to the scenario depicted above is the case of strongly self-gravitating clumps in (magneto-) hydrostatic equilibrium, from which the gas cannot escape once it has been captured (“decouples” from the intercloud medium). In this case, the cloud should be bounded by an accretion shock and, although strictly speaking there is flux across the shock, the accreted material is not mixed far beyond the shock into the cloud’s “body”. However, it seems to us that the question as to whether such quasi-hydrostatic configurations can actually be produced in a turbulent ISM remains open, as discussed in § 6.1.

3. Numerical Simulations

In the following sections, we discuss the topology of the density, velocity and magnetic fields in 2D numerical simulations of the ISM based on the model of Passot, Vázquez-Semadeni & Pouquet (1995) (hereafter PVSP95), which represents 1 kpc² of the ISM on the Galactic plane, centered at the solar Galactocentric distance. We refer the reader to that paper for the equations and parameters of the model, which includes self-gravity, magnetic fields, parameterized cooling and diffuse heating, the Coriolis force, large-scale shear, and parameterized localized stellar energy input due to ionization heating. The parameterized cooling is as in Chiang & Bregman (1988), who fitted piecewise power laws to the standard cooling calculations of Dalgarno & McCray (1972) and Raymond, Cox & Smith (1976). As discussed in VSPP96, the net result of the combined cooling and diffuse heating laws is that the flow effectively behaves as a polytrope, with an effective polytropic exponent γ_{eff} which is piecewise constant over the temperature range spanned by the flow. Alternatively,

it was shown in VSPP95 that, for the heating and cooling functions used there, the thermal equilibrium values of the temperature and pressure can be expressed as functions of the density in the range $100 \text{ K} < T < 10^5 \text{ K}$ for non star-forming regions. Therefore, γ_{eff} can also be expressed as a piecewise constant over the corresponding density range. For the fiducial values adopted in the model (PVSP95), γ_{eff} takes the values (VSPP96)

$$\gamma_{\text{eff}} = \begin{cases} 0.25 & 1.57 < \rho \text{ (} 100 < T < 2000 \text{)} \\ 0. & 0.39 < \rho \leq 1.57 \text{ (} 2000 \leq T < 8000 \text{)} \\ 0.48 & 3.15 \times 10^{-3} < \rho \leq 0.39 \text{ (} 8000 \leq T < 10^5 \text{)} \\ 3.3 & 4.28 \times 10^{-2} < \rho \leq 3.15 \times 10^{-3} \\ & \text{(} 10^5 \leq T < 4 \times 10^7 \text{),} \end{cases} \quad (4)$$

where densities are in units of cm^{-3} and temperatures in Kelvins. In eq. (4), equilibrium temperature ranges equivalent to the specified density ranges are indicated in parentheses. In the simulations, stellar ionization heating is modeled by means of a local heating source which is turned on if the density exceeds a critical value $\rho_c = 30\langle\rho\rangle$, where the brackets denote an average over the whole volume of the simulation. Note that temperatures over a few $\times 10^4 \text{ K}$ are never reached in the simulations, because supernovae are not included, since these require non-trivial modifications to the code (Gazol & Passot 1998). The maximum densities reached in the simulations are $\sim 100 \text{ cm}^{-3}$, with $T \sim 100 \text{ K}$.

The simulations we use are refinements of the PVSP95 model at a higher resolution (800×800 grid points), presented in Vázquez-Semadeni, Ballesteros-Paredes, & Rodríguez (1997), hereafter VSBPR97. The stellar energy injection maintains the turbulence in the medium, promoting further cloud formation. Nevertheless, we turn off star formation shortly before the time at which the data are analyzed, in order to allow for the largest possible density gradients, since otherwise the stellar heating prevents the density from reaching values significantly larger than ρ_c , by causing the neighboring gas to re-expand. The various physical quantities are in units of $\rho_0 = 1 \text{ cm}^{-3}$, $u_0 = 11.7 \text{ km s}^{-1}$, $T_0 = 10^4 \text{ K}$ and $B_0 = 5 \mu\text{G}$ (see PVSP95).

We have developed a cloud-finding numerical algorithm in physical space (as opposed to the position-velocity space of observational data) for the density data from the simulations (Ballesteros-Paredes and Vázquez-Semadeni 1995). A cloud is defined as a connected set of points (pixels) whose densities are

larger than a given threshold ρ_T . The clouds obtained through this procedure are clearly quite arbitrary, since as ρ_T is increased the boundary of the cloud simply moves “inwards”. However, eventually an increase in ρ_T will lead to a more qualitative change in which a given cloud splits into two or more “children”, in a similar manner to the “structure trees” used by Houllahan & Scalo (1992). This procedure is in a sense analogous to performing observations using different tracers sensitive to different density ranges. Alternative cloud identification algorithms based on locating density maxima (e.g., Williams, de Geus & Blitz 1994) were not investigated, but we do not expect that such procedures would affect the qualitative nature of our results, which, as will be seen, appear to follow quite generally from the physics of the problem.

Given the above algorithm for defining the clouds, the kinetic terms entering the VT are then evaluated numerically for each cloud, having previously subtracted its bulk mass-averaged velocity, defined as

$$\langle u_i \rangle_{\text{mass}} \equiv \frac{\int_V \rho u_i dV}{\int_V \rho dV}, \quad (5)$$

in order to measure only the contribution associated to the fluctuations. We refer to this as measuring the velocities in the “cloud frame”.

4. Results and Discussion

4.1. Density and velocity field topology

In figs. 1a, b and c we show three hierarchical levels of the density field (gray scale), with the corresponding velocity fields (arrows). In fig. 1c we further denote super- and sub-Alfvénic velocities with black and white arrows, respectively (see § 5), where the Alfvén speed is defined as $v_a^2 = B^2/\rho$ in the code’s units.

Figure 1a shows a snapshot of the simulation at $t = 7.2 \times 10^7 \text{yr}$. The density field ranges from ~ 0.01 to $\sim 100 \text{cm}^{-3}$. Figs. 1b and c show two subsequent hierarchical levels of clouds, obtained at $\rho_T = 4$ and 8, respectively. The sizes of the boxes shown in the three panels are 800, 215 and 45 pixels per side (1 pixel = 1.25 pc). We refer to the cloud in fig. 1b as the “parent” cloud, and to that in fig. 1c as the “child” cloud. Note that only fig. 1c shows the velocity field in the cloud frame.

Inspecting the plotted density and velocity fields, we observe that the fluid velocity at the cloud boundaries is in general continuous, at any level of the hi-

erarchy. Sharp changes in the velocity field (shocks)¹ are in general oblique and tend to occur mostly at the centermost parts of the clouds, where the highly filamentary density field exhibits “ridges”. This indicates that the density features are produced by colliding streams, a fact that can be seen more accurately in figs. 2a, b and c. These show cuts, along the x - (at $y = 514$, fig. 2a) and y - (at $x = 602$ and $x = 614$, figs. b and c respectively) axes, of the density ρ (solid line), and the x - and y -components of the velocity, u_x (dotted line) and u_y (long dashed line) for a region containing the clouds of figs. 1b and c. The axes in these plots indicate pixel number. For added clarity, we show in fig. 3 the lines along which these cuts are taken.

The central parts (3-5 pixels) of the density peaks are seen to correspond in general to large negative longitudinal gradients $\partial u_i/\partial x_i$ (no sum over i) of the velocity, i.e., shocks. However, the clouds (i.e., large density values) extend beyond the shocks for many more pixels, where the velocity component exhibits plateaus with superimposed small-scale structure. These plateaus are indicative of the approaching streams (extended inward motions). As an example, consider the peaks labeled “1” and “2” in fig. 2a. Peak 1 corresponds to a shock at $x = 602$, and is flanked by an expansion wave ($\partial u_x/\partial x > 0$) on the left, and by a plateau with $u_x < 0$ on the right, although the plateau itself contains substructure. This peak also corresponds to a shock along the y -direction (fig. 2b). Interestingly, peak “2” in fig. 2a does not seem to correspond to a shock along the x -direction, but in fig. 2c it can be seen that it is caused by a shock in the y -direction. In order to further illustrate this point, in fig. 3 we show the same cloud as in fig. 1c, but showing the density field as a gray-scale image and the divergence $\partial u_i/\partial x_i$ of the velocity field with contours. Local density maxima clearly coincide with local (negative) minima of the divergence.

It is worth noting that in figs. 2a, b and c, larger-scale density features are also seen to correspond to large-scale negative gradients of the velocity field, although with much substructure. See, for example, the large cloud complex (multiple density peak) extending from $580 \lesssim x \lesssim 680$ in fig. 2a. The very largest-scale inward flows are probably of gravitational rather than turbulent origin (e.g., Vázquez-Semadeni & Pas-

¹In the simulations, shocks are sharp gradients extending over 3 to 5 pixels, due to the action of viscosity (VSBPR97)

sot 1998), because the simulations do not include supernovae which could induce turbulent motions at those scales, but in the real ISM both cases are likely to occur.

There also appears to be a certain amount of spatial correlation between density and vorticity features. In figure 4 we show the vorticity field (contours) superposed onto the density field (gray-scale) for the cloud of fig. 1c. In this case, the correlation between local maxima of the density field and maxima (or minima) of the vorticity field is not as tight, the critical points of the vorticity being shifted by a few pixels with respect to the density peaks. Nevertheless, there is still a clear correspondence between vorticity and density features. This correlation can be understood because, as mentioned above, the stream collisions are in general oblique. It is possible then that the detailed structure inside the clouds consists of shocks and tangential discontinuities. Moreover, the shocks are generally curved and are encountering density variations in the pre-shock gas, so vorticity production is expected behind them (Hayes 1957; Passot & Pouquet 1987; Kornreich & Scalo 1998).

The continuity of the velocity field through the cloud boundaries has an interesting subjective implication. The definition of a cloud by a density threshold is actually seen to be rather arbitrary, since the clouds do not have sharp physical boundaries. Thus, as long as the change in the density threshold does not imply a “splitting” of a cloud into its offspring, it only amounts to considering the same cloud out to different distances from the maximum, but without there being any clear “edge” to the cloud. Note that this need not be in conflict with observations suggesting that molecular clouds have sharp edges (Blitz 1991), since in this case the observed boundaries may just reflect a transition from molecular to atomic gas, without a discontinuity in the gas mass density (e.g., Goldsmith 1987, Blitz 1991).

4.2. Virial surface terms and pressure confinement

The velocity fields observed in the simulations indicate a strong flux of the relevant dynamical quantities through the cloud boundaries at all scales. To quantify this, in fig. 5 we show a plot of the kinetic energy \mathcal{E}_{kin} vs. the kinetic surface term \mathcal{T}_{kin} for the parent complex shown in fig. 1a and all its daughter clouds resulting from setting $\rho_{\text{T}} = 4, 8, 11$ and 16, and with areas larger than 300 pixels. The latter requirement

is imposed in order to avoid including clouds so small that they are strongly influenced by viscous and diffusive numerical effects. The clouds shown in figs. 1b and c are represented with a different symbol in fig. 5 for identification. Note that both kinds of virial terms are computed in the cloud frame.

It is seen that in general the surface kinetic virial term is of the same order of magnitude as the volume term, i.e., the kinetic energy contained in the cloud’s volume. This means that both terms are of similar importance in shaping and supporting the clouds. At a more detailed level, this seems to be a reflection of the continuity of the velocity field. The flow is entering the clouds, and shocking at their innermost regions. Thus, the two terms refer to essentially the same process, only measuring it at different places (one over the cloud’s volume, the other at the cloud’s boundary but weighted by the distance to the center of mass), explaining their similar values. This is analogous to the well known property of the surface and volume thermal pressure terms, that if the pressure is constant the two terms cancel.

It is important to remark that the similarity between these two terms does not imply that the cloud is “confined” by turbulent pressure, in the sense that this is not a static configuration. First, the two terms do not cancel each other exactly, leaving a net contribution available for shaping the cloud (the contribution $\mathcal{E}_{\text{kin}} - \mathcal{T}_{\text{kin}}$ to d^2I/dt^2). Second, it is important to note that the points in fig. 5 lie sometimes above and sometimes below the line $\mathcal{E}_{\text{kin}} = \mathcal{T}_{\text{kin}}$, indicating that for some clouds the contribution to d^2I/dt^2 is positive, but negative for others. This implies that the kinetic terms sometimes provide net “support” and sometimes cause net compression, although in general the clouds are expected to suffer distortions that cannot be classified as either one of the above. Thus, the clouds are evolving with time, continuously changing their volume and shape, since they are the density fluctuations produced by the turbulence².

The thermal pressure, as discussed in VSPP95, shows little spatial variation (except near star formation sites where it is much larger) because $0 \leq \gamma_{\text{eff}} < 1$ in general for the temperature range spanned by the simulations. In particular, $\gamma_{\text{eff}} = 0$ implies an isobaric

²See the accompanying video to VSPP95 for a non-magnetic example. An mpeg video of a fully MHD simulation from PVSP95, among others, can be seen at <http://www.astroscu.unam.mx/turbulence/movies.html>

medium. Note that $\gamma_{\text{eff}} < 1$ is in agreement with the elementary fact that in the ISM denser regions are colder in that temperature range (Myers 1978). In other words, the near constancy of the pressure in this temperature range is a consequence of thermal balance (giving $\gamma_{\text{eff}} < 1$) in a medium whose density is determined by the turbulent motions. However, this near “pressure equilibrium” has no effect in confining the clouds, which are in a state of constant change. As stated in VSP95, the pressure is *slaved* to the density field, which in turn is determined by the turbulence.

4.3. Super- and sub-Alfvénic motions and magnetic field topology

Another point worth discussing is the sub- or super-Alfvénic character of the velocity, since it has been traditionally argued that the motions in molecular clouds are supersonic but sub-Alfvénic (e.g., Shu, Adams & Lizano 1987), although more recently it has been claimed by Padoan & Nordlund (1998) that this may not be so, but rather that motions may generally be super-Alfvénic. Since in our simulations clouds form out of the general ISM, they represent a good test to see which of these conditions develop, rather than using some pre-determined assumption about the sub- or super-Alfvénic character of the problem (e.g., Mouschovias 1987; Lizano & Shu 1989). In fig. 1c the black and white arrows respectively denote super- and sub-Alfvénic velocities. It is seen that *inside the cloud there are both sub- and super-Alfvénic velocities*. Since the velocity field does not show large magnitude fluctuations at the transition sites, this can only be understood in terms of a change in the Alfvén speed v_a . To see this, in fig. 1c contours of the magnitude B of the magnetic field are shown as well. The contours span the range from 4 to 10 μG , in intervals of 1.5 μG . Thicker lines indicate progressively larger values of B . The velocity is seen to be sub-Alfvénic everywhere outside the cloud. Inside the cloud, it is super-Alfvénic in the lower region of the cloud. In the upper region, the velocity is sub-Alfvénic due to a combination of large B -values and low densities. Looking down towards the center, another super-Alfvénic region is seen, due mainly to the increase in the density, which reaches $\rho = 55 \text{ cm}^{-3}$ at the peak. However, at the peak, the velocity becomes sub-Alfvénic again, this time due to a sharp decrease in the velocity magnitude itself – sort of a “stagnation point” at the density peak. These vari-

ations are thus due again to the collisions between the magnetized gas streams, which push the field and cause magnetic shocks and field reversals where the fluid shocks occur, and in general produce a rather chaotic flow. One such reversal is seen to occur on the filament extending out of the cloud towards the lower left corner of fig. 1c. This is seen on the contours as a decrease in the field’s intensity towards the central ridge of the filament. Figure 4, which shows the magnetic field vectors on top of the density (gray scale) and the vorticity (contours), shows this phenomenon more clearly.

Note that this trans-Alfvénic character of the motions may explain why the density peaks are “fat” compared to the stream-collision sites: the information of the presence of the collision is often able to travel upstream of the flow. Furthermore, since the collisions are generally oblique, it is likely that magnetosonic waves propagating perpendicular to the collision surface may overtake the perpendicular component of the oblique fluid motion, even if the total fluid velocity is super-Alfvénic. In contrast, it is well known that in Burgers turbulence, where no pressure is available, the density structures are as thin as allowed by viscosity exclusively (see, e.g., Chappell & Scalo 1998).

The advection of the magnetic field described above is contrary to the usual assumption that the field controls the fluid motions, forcing the gas to flow along the field lines. Nevertheless, it is noteworthy that the field strengths developed by the simulations in both the intercloud medium and in the clouds are not unrealistic. The lowest values of the field occur at the intercloud medium, and are $\sim 1\mu\text{G}$, while the largest values occur in the densest regions, with values $\sim 25\mu\text{G}$. Nevertheless, the field is quite intermittent, and does not follow a unique scaling with the density (PVSP95), exhibiting significant variations within the cloud of fig. 1c. Moreover, even under near-equipartition conditions between kinetic and magnetic energy, the velocity field should be expected to exert as much of an influence on the magnetic field as viceversa. In § 5.2 we discuss the degree to which this field topology is consistent with observations.

5. Comparison with observations.

The scenario presented here differs significantly from the standard view in which clouds and clumps have well defined boundaries (density discontinuities)

which separate them from a much more tenuous, warmer medium, as in simulations of cloud collisions (e.g., Pumphrey & Scalo 1983; Klein et al. 1995; Miniati et al. 1997), of cloud confinement (e.g., BM92), quasi-static contraction (e.g., Lizano & Shu 1989) and stability (e.g., Ebbert 1955; Bonnor 1956; McLaughlin & Pudritz 1996), etc. On the other hand, Scalo (1990) has suggested that such a standard model may be an over-idealization stemming from the low resolutions and column density ranges of early studies, and proposed instead a much more complex scenario in which clouds do not have a well-defined identity. Our results support this view, and in fact such poorly-defined identity is reflected in the arbitrariness of cloud- and clump-finding algorithms (e.g., Williams, de Geus & Blitz 1994; VSBPR97). It is necessary, however, to test whether the scenario proposed here is consistent with different observations.

5.1. Comparison between observed spectral-line maps and mass-weighted velocity histograms

The colliding streams we have described as responsible for cloud formation should manifest themselves as multiple peaks in density-weighted velocity histograms of one velocity component, the equivalent in our simulations of the optically thin line profiles in observational spectral line maps. Although frequently Gaussian or other smooth curves are used to fit such lines, conferring the idea that the lines are unimodal and correspond to well-defined, isolated entities, in actuality the profiles generally exhibit multiple peaks (for recent examples, see, e.g., Falgarone et al. 1994 etc.) which are in fact normally interpreted as “clumps” (e.g., Williams, Blitz & Stark 1995, hereafter WBS95).

For comparison with observational profiles, we show in fig. 6 the density-weighted histogram of the x -component of the velocity (u_x) for the “parent” cloud showed in fig. 1b. As usual, this histogram has been obtained using the local speeds in the cloud frame. This histogram may be compared with the ^{13}CO line profile for the Rosette Molecular Cloud (RMC) shown in fig. 4 of WBS95³. This cloud is in many aspects comparable to the cloud of fig. 1b: while the RMC’s dimensions (as deduced from fig. 17 in WBS95) are

$\sim 90 \times 70$ pc, the cloud in fig. 1b is $\sim 250 \times 120$ pc. Furthermore, the cloud in fig. 1b has a mean density of $\sim 10 \text{ cm}^{-3}$, while the gas sampled in the spectrum of fig. 4 of WBS95 has a mean density $\sim 15 \text{ cm}^{-3}$.

Comparing the histograms for both of these clouds, we note several points in common. First, both sets of data have FWHMs of roughly 6 km s^{-1} when only the main features are considered. Second, both sets exhibit high-velocity bumps, at several km s^{-1} from the centroid. Finally, and probably most importantly, the “main” features are seen to contain substructure in both sets of plots. However, while such features have been traditionally interpreted as “clumps”, in our simulations they originate from extended regions within the cloud.

In order to explain this phenomenon, we show in fig. 7 a different representation of the parent cloud (fig. 1b). The isocontours denote the density field, the arrows show the velocity field in the frame of the cloud, and the various tones of gray represent zones with nearly the same x -component of the velocity u_x . The velocities range from less than -8 km s^{-1} to more than 8 km s^{-1} . Each tone of gray indicates a velocity interval of 2 km s^{-1} . Several issues are then observed. First, we note that the various peaks in the histogram of fig. 6 contain contributions from extended and separate regions in space. Second, local density peaks often encompass several velocity intervals, in a similar fashion to the situation for the entire cloud, suggesting a kind of self-similarity. Note then that the relative height in the histogram depends mainly in the mass fraction of the gas with the corresponding value of u_x , since every velocity interval appears to sample a wide range of densities. Third, a given feature (peak) in the histogram may have contributions from regions with very different total velocity vectors, which only happen to have a similar x -component. The above results suggest that the identification of “clumps” as features in velocity space is risky at best, and possibly erroneous, as already pointed out by Adler & Roberts (1992).

A final word concerning the velocity field is in order. As pointed out in § 4.1, significant vorticity is found within the clouds. Observationally, this may be detected as velocity gradients along the cloud’s projected area on the sky, which indeed have been observed (e.g., Arquilla & Goldsmith 1986; Goodman et al. 1993). Furthermore, Miville-Deschênes, Joncas & Falgarone (1998) have recently reported possible direct evidence for vorticity in clouds.

³Although fig. 4 in WBS95 shows CO spectra, which are optically thick, there is little, if any, qualitative difference with the optically thin ^{13}CO spectra shown in fig. 5 of that paper

5.2. Magnetic Field: alignment, advection and field reversals

Concerning the magnetic field topology, the field reversals and bendings mentioned in § 4.3 might seem contrary to the widely accepted fact that the magnetic field lines projected on the plane of the sky, as obtained in polarization analysis (see, e.g., Goodman et al. 1990), are relatively smooth over the area of the clouds. However, on closer inspection of the field topology in our simulations, there is no contradiction. As can be seen in fig. 4, the magnetic field bendings are correlated with bendings of the density features, so that, along elongated density features, the field appears rather smooth. Besides, the projection along the line of sight can make the field lines appear smoother than they are (Ballesteros-Paredes and Vázquez-Semadeni 1998). On the other hand, evidence that the interaction of a shock with dense molecular gas is producing a reversal in the line-of-sight field component in the Orion/Eridanus region has been recently reported (Heiles 1997).

Note also that it is by now well established that the field lines do not in general show a unique direction of alignment with the density features (Goodman et al. 1992). In our simulations this is also true. Although in particular for the case shown in fig. 4 the field lines are mostly parallel to the density features, in other cases they are perpendicular (see, e.g., the concave region at coordinates $x \sim 605$ and $y \sim 510$ in fig. 4).

5.3. Lifetimes of turbulent clouds

An important consideration is whether the turbulent-fluctuation nature of the clouds proposed here gives cloud lifetimes consistent with current estimates. First of all, we should point out that clouds are not necessarily completely disrupted by the turbulence. Frequently they are simply sheared, split, merged with others, or they can just re-expand into the general medium if they are not very strongly self-gravitating, again indicating that the medium is not in precise pressure balance (see the videos mentioned above).

In any case, a conventional estimate for a typical “lifetime” can be given by $\tau = l/\Delta v$, where l is a characteristic size of the cloud and Δv its internal velocity dispersion. As an example, we calculate this for the “daughter” cloud of fig. 1c. We find $\Delta v = 2.3$ km s⁻¹, and $l \sim 30$ pixels = 37.5 pc. Thus, $\tau \sim 1.6 \times 10^7$ yr. This value is consistent with various estimates of GMC lifetimes of order a few $\times 10^7$ yr

(Bash, Green & Peters 1977; Blitz & Shu 1980; Larson 1981; Blitz 1994).

6. Discussion

6.1. Applicability to molecular gas and the role of γ_{eff}

The analyses from the previous sections have been performed on simulations which have reasonably realistic cooling functions and a diffuse heating which decays with increasing density (mimicking self-shielding) (PVSP95). As seen from eq. (4), such heating and cooling rates imply effective polytropic exponents typically smaller than 1. These heating and cooling rates are most appropriate for diffuse HI structures, which may be very large (up to ~ 1 kpc, although small-scale structure must exist there as well). The question then arises as to whether the dynamical scenario we have proposed here is applicable to molecular clouds (MCs) and their substructure (with sizes ~ 10 to $\lesssim 0.1$ pc). Although the ultimate test for this problem will require new numerical simulations, which will be presented elsewhere, we can discuss the issue to a certain extent here, based on recent results on the role of γ_{eff} (Tohline et al. 1987; VSPP96; Passot & Vázquez-Semadeni 1998), which is a measure of the thermal characteristics of the flow.

The main difference between the parameters of the simulations presented here and another set more appropriate for MCs is the effective polytropic exponent of the flow. (Note that the only scale-dependent quantities in our simulations are the heating and cooling rates. All other quantities are scale-free.) While in general in our simulations $0 \leq \gamma_{\text{eff}} < 0.5$ (c.f. § 3), it is possible that in molecular gas $\gamma_{\text{eff}} \gtrsim 1$ (Myers 1978). Actually, the situation at densities $\gtrsim 10^3$ cm⁻³ is rather uncertain, with γ_{eff} possibly being ~ 1 between 10^3 and a few $\times 10^4$ cm⁻³ because of the importance of collisional deexcitation and radiative trapping in CO lines, and either larger or smaller than unity at larger densities depending on the presence of embedded stellar sources and other factors (Scalo et al. 1998).

In any case, we can discuss the expected effect of the gas having $\gamma_{\text{eff}} \gtrsim 1$ on the nature of the density fluctuations arising in the flow. It has recently been shown by Passot & Vázquez-Semadeni (1998) that at larger γ_{eff} the density peaks are spatially more extended and of smaller amplitude, while the density minima are very deep. At small γ_{eff} (typ-

ically $0 \leq \gamma_{\text{eff}} \leq 1$), the situation is reversed, the peaks being very concentrated and large, while the minima are not as deep. This is because the sound speed c scales with the density as $\rho^{(\gamma_{\text{eff}}-1)/2}$, causing the peaks to re-expand faster at larger γ_{eff} . At $\gamma_{\text{eff}} = 1$ a critical case occurs, the fluctuations of $\ln \rho$ being symmetrical with respect to the mean. VSPP96 have calculated the density jump for shocks in a barotropic fluid parameterized by γ_{eff} . Thus, if γ_{eff} is larger at MC densities than in our simulations, we can expect the density peaks to be wider and less pronounced. But we do not expect the general scenario of clumps being formed by turbulent compressions to change significantly. The colliding streams, if supersonic (or super-magnetosonic), create non-stationary shock-bounded slabs, which simply re-expand (if not made self-gravitating by the compression—see below) on different timescales depending on γ_{eff} after the compression subsides. If the compressions are subsonic no shocks form, but, for sufficiently small γ_{eff} and/or cloud masses close to their Jeans mass, collapse may still be induced by the compressions (Tohline et al. 1987).

One crucial issue, however, is whether the compressed slabs can become self-gravitating upon the compression, and, if so, whether a quasi-hydrostatic configuration can be formed. The former problem has been addressed by a number of authors (Hunter 1979; Hunter & Fleck 1982; Tohline et al. 1987; Vishniac 1983, 1994; Elmegreen 1993b; VSPP96). Two main issues are at play here. One is the total gravitational (E_g) and internal (E_i) energies of the cloud (for the purpose of this discussion the “internal” energy can be generalized to include all forms of energy that provide support for the cloud against gravity). The other is the *rate* at which each energy increases upon compression. If $|E_g| > E_i$, the cloud is gravitationally unstable, and collapses upon a perturbation. This is essentially an integral version of the Jeans criterion (e.g., Bonazzola et al. 1987). However, for three-dimensional collapse, it is well-known that, if $\gamma_{\text{eff}} > \gamma_{\text{cr}} \equiv 4/3$, then the collapse will ultimately be halted, since E_i increases faster than $|E_g|$. The corresponding values of γ_{cr} for 2- and 1-dimensional collapse are respectively 1 and 0 (VSPP96).

Conversely, if a cloud is initially stable according to Jeans ($E_i \geq |E_g|$), it may be made unstable upon compression. Tohline et al. (1987) have calculated the required Mach number of a 3-dimensional compression as a function of γ_{eff} for this to occur, pro-

vided that $\gamma_{\text{eff}} < 4/3$ (for $0 < \gamma_{\text{eff}} < 1$ they found that the required Mach number is independent of the cloud’s mass). Two- and one-dimensional compressions require $\gamma_{\text{eff}} < 1$ and $\gamma_{\text{eff}} < 0$, respectively (VSPP96). The issue is then the following. In order for an initially stable cloud to be pushed over the internal energy “barrier” (Tohline et al. 1987) by a strong enough turbulent compression, it is necessary that $\gamma_{\text{eff}} < \gamma_t$, where γ_t is the critical γ for $|E_g|$ to increase faster than E_i upon the turbulent compression. From there on, gravitational collapse takes over. Since in general turbulent compressions are expected to be less than three-dimensional, then generally we expect $\gamma_t \leq \gamma_g$, where γ_g is the critical γ for gravitational collapse.⁴ Then, $\gamma_{\text{eff}} < \gamma_t \leq \gamma_g$. Thus, we conclude that, if collapse was triggered by a turbulent compression, it cannot later be halted by the internal energy, unless γ_{eff} changes in the process. The latter may happen in the late stages of collapse, if the dynamical timescales become shorter than the radiative cooling timescales, causing γ_{eff} to approach the actual heat capacity ratio of the gas γ , rather than the value derived from the condition of thermal equilibrium (see, e.g., PVSP95).

We should insist here that the effects of all forms of support, such as the magnetic pressure and turbulent support, can in principle be included in γ_{eff} . On the other hand, this is a very simplistic description, since in general γ_{eff} may be a function of the density, and the anisotropic nature of magnetic support may not be well described by a simple polytropic exponent. In any case, this discussion illustrates our main point: *quasi-hydrostatic configurations cannot be produced out of turbulent fluctuations, unless the flow becomes closer to adiabatic than to isothermal during the collapse.* Fluctuations either rebound or collapse. However, at small γ_{eff} , the rebound time is long (VSPP96; Passot & Vázquez-Semadeni 1998).

We can examine more quantitatively the conditions under which adiabatic compression or collapse would occur if thermal pressure provides the main support mechanism for a clump, by comparing the cooling timescale $\tau_{\text{cool}} = nkT/\Lambda$ (Λ = cooling rate in units of $\text{erg cm}^{-3} \text{s}^{-1}$) to the compression time $\tau_{\text{comp}} \equiv L/v$ and the collapse time $\tau_{\text{coll}} \equiv (G\rho)^{-1/2}$. For the cooling rate we distinguish two density regimes. For

⁴Here we are allowing for the possibility of gravitational collapse to occur faster in one direction than in the other two, as is the case of cosmological “pancakes”.

$10^3 \lesssim n \lesssim 10^4 \text{ cm}^{-3}$ the cooling is dominated by CO line cooling. We adopt a rough approximation for the CO cooling rate (see references in Scalo et al. 1998) as $\Lambda \sim 10^{-26} n_3 T^2$, where $n_3 = n/10^3 \text{ cm}^{-3}$ and we have assumed that collisional deexcitation yields a linear (rather than quadratic) density dependence at these densities. We recognize that this is a crude representation of the molecular cooling rate, but it suffices for our order of magnitude estimates. At larger densities the cooling will be dominated by gas-grain collisions (if there are no embedded protostellar sources), with a rate $2 \times 10^{-33} n^2 T^{1/2} (T - T_{\text{gr}})$, where T_{gr} is the grain temperature and the coefficient depends somewhat on the adopted grain parameters. We assume $T - T_{\text{gr}} \approx T$ for our order of magnitude estimates.

For compressions, we find that the condition for adiabatic evolution ($\tau_{\text{comp}} < \tau_{\text{cool}}$) yields a critical length scale $L_{\text{pc}} = L/1\text{pc}$

$$L_{\text{pc}} < \begin{cases} 4 \times 10^{-3} M / T_{10}^{1/2} & \text{CO cooling} \\ 7 \times 10^{-4} M / n_5 & \text{gas-grain cooling,} \end{cases}$$

where M is the Mach number of the compression, $T_{10} = T/10\text{K}$, and $n_5 = n/10^5 \text{ cm}^{-3}$. For any reasonable Mach number adiabatic compression is only possible for tiny regions of size $\lesssim 10^{-2} \text{ pc}$.

If a (non-adiabatic) compression results in collapse, the condition for adiabatic collapse is $\tau_{\text{coll}} < \tau_{\text{cool}}$. At densities $10^3 \lesssim n \lesssim 10^4$, the adopted CO cooling rate results in the condition $n_3 > 2.1 \times 10^3 T_{10}^2$. But at such large densities the cooling will be controlled by gas-grain collisions, not molecular line cooling. Using the gas-grain cooling rate, the condition for adiabatic collapse is found to be $n_5 < 1.2 \times 10^{-3} T_{10}^{-1}$. But at such small densities molecular line cooling would dominate and be non-adiabatic. Thus for collapse induced by compression, adiabatic evolution will never occur until the collapsing entity is so dense that it becomes opaque to its own infrared radiation, which only occurs at very large (protostellar) densities.

These estimates indicate that turbulence-induced compressions or collapse will generally be controlled by the effective polytropic index γ_{eff} set by the thermal equilibrium condition, since τ_{cool} is smaller than the relevant dynamical timescales, except for extremely small scales of compression or at protostellar densities for collapse. We conclude that quasi-static configurations are unlikely over a very wide range of physical parameters.

Is there any observational evidence for a dynamical

rather than quasistatic state of clumps? A preliminary answer appears affirmative. Indeed, Girart et al. (1997) have recently reported on a system which may be interpreted as a collision of streams in L723. Furthermore, Tafalla et al. (1998) have reported a core with inward motions that do not correspond to classical gravitational infall models. A detailed comparison of these data with our scenario will be presented elsewhere.

6.2. Effect of dimensionality

In this paper we have used two-dimensional simulations, with the known risks involved by them, such as a different distance dependence of gravity, the absence of a magnetic dynamo, and the possibility of reverse cascades (although this is probably less important in the compressible case, where the energy spectrum may be determined by the shocks rather than by cascade processes – see, e.g., Vázquez-Semadeni 1998). This is a necessary price to pay for the larger resolution allowed by the two-dimensionality, which is essential for the type of hierarchical structure analyses performed here.

However, we do not expect the two-dimensionality of our simulations to be a matter of concern for the validity of our results. The main points raised here are those of the mechanism of cloud formation and its consequences regarding the mass flux through cloud boundaries, the deformation of the magnetic field by the flow, and the interpretation of line profile observational data. These do not seem to depend on the dimensionality of the problem, since they originate from the shocks and collisions of streams, which occur in both two and three dimensions. In any case, intermediate-resolution 3D simulations are currently being performed which will allow us to test these expectations.

7. Summary and conclusions

In this paper we have conducted a close examination of the topology of the density, velocity and magnetic fields that result in our 2D simulations of the ISM at the kpc scale, in particular within the clouds that emerge as the turbulent density fluctuations in that medium. We found that, in general, the cloud boundaries are rather arbitrary, being defined only by a density threshold criterion, but not by a physical boundary, such as a density or velocity discontinuity. The same arbitrariness is likely to be present

in clouds defined by the tracer used to observe them, since a cloud may seem to “end” where the tracer density falls below a threshold density necessary to excite the transition, but this need not correspond to any abrupt drop in the mass density.

We furthermore considered a hierarchy of clouds in the simulations, by using a sequence of three progressively larger density thresholds for defining them. For clouds at all levels of this hierarchy, the velocity field in the simulations is continuous across the clouds’ “boundaries”, indicating that the clouds are being formed by colliding gas streams (Hunter et al. 1986; Elmegreen 1993b; VSPP95), with the density increasing towards the collision site. The density enhancements need not be confined exclusively to the collision site as in Burgers flows, because the velocities involved are typically trans-Alfvénic, meaning that the information on the collision can often propagate upstream (see also Pouquet, Passot & Léorat 1991). Furthermore, since the collisions are generally oblique, it is likely that magnetosonic waves propagating perpendicular to the collision surface may overtake the oblique fluid motion, even if the total fluid velocity is super-Alfvénic. This scenario is in sharp contrast with static models in which the clouds are immersed in an intercloud medium of lower density but higher temperature, and confined by pressure balance between the two “phases” (e.g., BM92; MZ92; McLaughlin & Pudritz 1996). In our simulations both “phases” exist, but the transition between them is smooth, and the situation, rather than being static, is highly dynamic.

To further characterize the role of the flux across the clouds’ boundaries, we considered the surface (\mathcal{T}_{kin}) and volume (\mathcal{E}_{kin}) kinetic terms in the virial theorem for the whole ensemble of clouds at one temporal snapshot in the simulation. It was found that both terms are typically of the same order of magnitude, indicating that the surface terms contribute an amount comparable to the total kinetic energy of the clouds to their overall virial balance. This was interpreted as a signature of the fact that, when the clouds are formed by stream collisions, the same flow is responsible for both the total kinetic energy contained within the clouds and for the flux across its boundaries.

We discussed the differences between the thermal and turbulent pressures, emphasizing the fact that while the former is microscopic and isotropic, the latter may involve macroscopic scales, comparable or

even larger than the clouds’ sizes, and is in general anisotropic, as indicated by its off-diagonal contribution to the total pressure tensor Π_{ij} . We thus concluded that turbulent pressure confinement is a contradictory concept, because it involves motions at large scales which by definition cause a change in the clouds’ boundaries. In turn, we argued that thermal pressure equilibrium in a non-static medium is irrelevant, because inertial motions may still distort or disrupt a cloud, even under thermal pressure balance with its surroundings.

Additionally, we studied the magnetic field topology and strength in the clouds in the simulations, and their implication on whether the motions are super- or sub-Alfvénic, finding both super- and sub-Alfvénic motions within the clouds, supporting the suggestion that the field is highly intermittent (Padoan & Nordlund 1998). We noticed that the field is significantly distorted and advected by the flow, in agreement with the result that the flow within the clouds is trans-Alfvénic. The field tends to be correlated with the density features, although without a unique mode of alignment (PVSP95). This causes the field to look relatively smooth along density features, in agreement with most polarization studies (Goodman et al. 1990), but at the same time being bent where the density filaments are bent as well.

A crucial question is whether the scenario depicted in this paper is consistent with observational data. We addressed this problem at the level of density-weighted velocity histograms, which can be compared to observational spectral line profiles from real clouds of similar characteristics to those in the simulations. Although there are limitations to this comparison, our velocity histograms are encouragingly similar to the observational line profiles, both exhibiting comparable FWHMs ($\sim 6 \text{ km s}^{-1}$) and high-velocity isolated features, and both containing not completely resolved substructure, indicating multiple components. We emphasized that while this substructure is usually interpreted as isolated “clumps”, in our simulations it originates from different regions of the cloud, which may correspond to different “streams” and in general have one similar component of the velocity but very different total velocity vector, as found also by Adler & Roberts (1992). We also mentioned observational evidence for field reversals in shocks (Heiles 1997), and noted that the topology of the magnetic field seen in the simulations is consistent with observations (Goodman et. al 1992).

Finally, we discussed at considerable length the possibility that the scenario of clouds as turbulent density fluctuations may apply to molecular clouds and their substructure (clumps and cores). Essentially, only the adopted cooling and heating functions in our simulations distinguish them from a case more appropriate to molecular clouds, which are believed to behave in a nearly isothermal manner. Based on recent results on the effect of the effective thermal behavior (Tohline et al. 1987; VSPP96; Passot & Vázquez-Semadeni 1998), parameterized by the effective polytropic exponent γ_{eff} , we conjectured that only the shape (height and width) of the density fluctuations is expected to change, but not the general character of the inflowing streams characteristic of their turbulent nature. We also suggested that quasi-hydrostatic configurations cannot be produced from turbulent compressions, and that density fluctuations must either collapse or rebound, unless the effective thermal behavior becomes closer to adiabatic during the collapse ($\gamma_{\text{eff}} \geq 4/3$). However, for small γ_{eff} , the rebound times can be quite long. We demonstrated, using appropriate cooling rates, that adiabatic evolution, and hence quasistatic configurations, are unlikely to occur either during compressions or during compression-induced collapse.

In summary, we conclude this paper by stating that the results presented here are not in contradiction, but rather quite consistent, with observational data. They seem to be, however, discrepant with the standard interpretation of those data in terms of sharply-bounded clouds in pressure equilibrium with their surroundings, and with the identification of velocity features in spectral-line data with isolated “clumps”.

We thank Alyssa Goodman, Thierry Passot, Luis Rodríguez and Jonathan Williams for carefully reading the manuscript and providing us with detailed comments. We also thank Paola D’Alessio and Susana Lizano for useful discussions. We acknowledge the hospitality of the star formation group at the Harvard-Smithsonian CfA. The simulations were performed on the Cray Y-MP/4-64 of DGSCA, UNAM. This work has received partial support from grants UNAM/DGAPA IN105295 and UNAM/CRAY SC-008397 to E.V.-S. and a UNAM/DGAPA fellowship to J.B.-P.

REFERENCES

- Adler, D. S. & Roberts, W. W. Jr. 1992, *ApJ*, 384, 95
- Arquilla, R., & Goldsmith, P. F. 1986, *ApJ*, 303, 356
- Ballesteros-Paredes, J. & Vázquez-Semadeni, E. 1995. *Rev. Mex. A. Ap. Conf. Series* 3, 105
- Ballesteros-Paredes, J., & Vázquez-Semadeni, E. 1998, in preparation.
- Ballesteros-Paredes, J., Vázquez-Semadeni, E. C., Gazol, A., and Passot, T. 1998, in preparation.
- Bash, F. N., Green, N., & Peters, W. L., III. 1977, *ApJ*, 217, 464
- Bertoldi, F. & McKee, C. F. 1992. *ApJ* 395, 140 (BM92)
- Blitz, L., & Shu, F. H. 1980, *ApJ*, 238, 148
- Blitz, L. 1991, in *The Physics of Star Formation and Early Stellar Evolution*, ed. C. Lada and N. Kylafis (Dordrecht: Kluwer), p. 3.
- Blitz, L. 1994, in *The Cold Universe*, ed. T. Montmerle, C. J. Lada, I. F. Mirabel, & J. Tran Than Van (Gif-sur-Yvette: Frontiers), p. 99.
- Bonazzola, S. Falgarone, E., Heyvaerts, J., Pérault, M., & Puget, J. L. 1987. *A& A* 172, 293
- Bonnor, W. B. 1956. *ApJ* 116, 351
- Chandrasekhar, S. 1951, *Proc. R. Soc. London*, 210, 26
- Chandrasekhar, S. & Fermi, E. 1953. *ApJ* 118, 116
- Chappell, D., & Scalo, J. 1998, *ApJ*, in press.
- Chiang, W. H. & Bregman, J. N. 1988. *ApJ* 328, 427
- Chièze, J. P. 1987. *A& A* 171, 225
- Dalgarno A. & McCray, R. A. 1972. *ARA& A* 10, 375
- Ebbert, R. 1955. *Z. Astrophys.* 37, 222
- Elmegreen, D. M. & Elmegreen, B. G. 1978. *ApJ* 220, 510
- Elmegreen, 1993a. In *Protostars and Planets III*. Ed. E. H. Levy & J. I. Lunine. (Tucson: Univ. of Arizona Press), p. 97.

- Elmegreen, 1993b. *ApJL* 419, L29
- Falgarone, E. Phillips, T. G. & Walker, C. K. 1991. *ApJ* 378, 186
- Falgarone, E., Lis, D.C., Phillips, T. G., Pouquet, A., Porter, D. H. & Woodward, P. R. 1994. *ApJ* 436, 728
- Franco, J. & Carramiñana, A. 1998. *Interstellar Turbulence*. (Cambridge: University Press), in press.
- Fuller G. A., & Myers, P. C. 1992. *ApJ* 384, 523
- Gazol, A., & Passot, T. 1998, in preparation.
- Girart, J. M. Estalella, R., Anglada, G., Torrelles, J. M., Ho, P. T. P. & Rodríguez, L. F. 1997. *ApJ* 489, 734
- Goldsmith P. F. 1987, in *Interstellar Processes*, ed. D. J. Hollenbach & H. A. Thronson. (Dordrecht: Reidel), p. 51.
- Goodman, A. A., Bastien, P. Menard, F & Myers, P. C. 1990. *ApJ* 359, 363
- Goodman, A. A., Jones, T., Lada, E. A. & Myers, P. C. 1992. *ApJ* 399, 108
- Goodman A. A., Benson, P. J., Fuller, G. A. & Myers, P. C. 1993, *ApJ*, 406, 528
- Hayes, W. D. 1957. *J. Fluid Mech.* 2, 595
- Heiles, C. 1997. *ApJS*. 111, 245
- Houllahan, P. & Scalo, J. 1992. *ApJ* 393, 172
- Hunter, J. H. Jr. 1979, *ApJ*, 233, 946
- Hunter, J. H. Jr., & Fleck, R. C. 1982, *ApJ*, 256, 505
- Hunter, J. H. Jr., Sandford, M. T. II, Whitaker, R. W. & Klein, R. I. 1986. *ApJ*, 305, 309
- Keto, E. R. & Myers, P. C. 1986. *ApJ* 304, 466
- Klein, R. I., McKee, C. F., & Woods, D. T. 1995, in *The Physics of the Interstellar Medium and Inter-galactic Medium*, eds. A. Ferrara, C. F. McKee, C. Heiles, & P. Shapiro (San Francisco: Astronomical Society of the Pacific), p. 366.
- Kornreich, P. & Scalo, J. 1998, *ApJ*, in press.
- Landau, L. D. & Lifshitz, E. M. 1987, *Fluid Mechanics*, 2nd ed. (New York: Pergamon)
- Larson R. B. 1981. *M.N.R.A.S.* 194, 809
- Léorat, J., Passot, T., & Pouquet, A. 1990. *M.N.R.A.S.* 243, 293
- Lizano, S. & Shu, F. H. 1989. *ApJ* 342, 834
- Maloney, P. 1988. *ApJ* 334, 761
- Mc Cray, R. & Snow, T. P. Jr. 1979. *ARA& A* 17, 213
- McCrea, W. H. 1957. *MNRAS* 194, 809
- McKee C. F. & Zweibel, E., 1992. *ApJ* 399, 551 (MZ92)
- McLaughlin, D. E. & Pudritz, R. E. 1996. *ApJ* 469, 194
- Miniati, F., Jones, T. W., Ferrara, A., & Ryu, D. 1997, *ApJ*, 491, 216
- Miville-Deschênes, M.-A., Joncas, G., & Falgarone, E. 1998, in *Interstellar Turbulence*, eds. J. Franco and A. Carramiñana, (Cambridge: University Press) in press.
- Mouschovias 1987, in *Physical Processes in Interstellar Clouds*, ed. G.E. Morfill, M. Scholer (Dordrecht: Reidel), p. 453.
- Myers, P. C. 1978. *ApJ* 225, 380
- Myers, P. C., & Goodman, A. A. 1988a. *ApJL* 326, L27
- Myers, P. C., & Goodman, A. A. 1988b. *ApJ* 329, 392
- Padoan & Nordlund, 1998, *ApJ*, submitted
- Parker, E. N. 1969. *Space Science Reviews* 9, 651
- Parker, E. N., 1979. *Cosmical Magnetic Fields. Their Origin and Their Activity* (Oxford: University Press).
- Passot, T. & Pouquet, A. 1987. *J. Fluid Mech.* 181, 441
- Passot, T., Vázquez-Semadeni, E. & Pouquet, A. 1995. *ApJ* 455, 536 (PVSP95)
- Passot, T., & Vázquez-Semadeni, E. 1998, *Phys. Rev. E.*, in press.

- Pouquet, A., Passot, T. & Léorat, J. 1991, in Fragmentation of Molecular Clouds and Star Formation, ed. E. Falgarone, F. Boulanger & G. Duvert (Dordrecht: Kluwer), p. 101.
- Pumphrey, W. A., Scalo, J. 1983. ApJ 269, 531
- Raymond, Cox & Smith 1976. ApJ 204, 290
- Scalo, J. 1987, in Interstellar Processes, ed. D. J. Hollenbach & H. A. Thronson. (Dordrecht:Reidel), p. 349.
- Scalo, J. 1990. in Physical Processes in Fragmentation and Star Formation, ed. R. Capuzzo-Dolcetta, C. Chiosi & A. di Fazio. (Dordrecht: Kluwer), 151.
- Scalo, J., Vázquez-Semadeni, E., Chappel, D., & Passot, T. 1998. ApJ in press.
- Shu, F., Addams, F. C., & Lizano, S. 1987. ARA& A 25, 23
- Stevens, I. R., Blondin, J. M., & Pollock, A. M. T. 1992. ApJ 386, 265
- Tafalla, M., Mardones, D., Myers, P. C., Caselli, P., Bachiller, R., & Benson, P. J. 1998, ApJ, accepted
- Tohline, J. E., Bodenheimer, P. H., & Christodoulou, D. M. 1987, ApJ, 322, 787
- Torrelles, J. M., Rodríguez, L. F., Cantó, J., Carral, P., Marcaide, J., Moran, J. M., & Ho, P. T. P. 1983. ApJ 274, 214
- Vázquez-Semadeni, E. 1998, “Turbulence in Molecular Clouds”, in Chemistry, Physics, and Observations of Molecules in Space, ed. W. F. Wall, A. Carramiñana, L. Carrasco, & P. F. Goldsmith (Dordrecht: Kluwer), in press.
- Vázquez-Semadeni, E. Ballesteros-Paredes, J., & Rodríguez, L. F. 1997. ApJ 474, 292 (VSBPR97)
- Vázquez-Semadeni, E. & Gazol, A. 1995. A& A 303, 204
- Vázquez-Semadeni, Passot & Pouquet, 1995. ApJ 441, 702 (VSPP95)
- Vázquez-Semadeni, E., Passot, T. & Pouquet, A. 1996. ApJ 473, 881 (VSPP96)
- Vázquez-Semadeni, E. & Passot, T. 1998, in Interstellar Turbulence, ed. J. Franco, J. & A. Carramiñana (Cambridge: University Press), in press.
- Vishniac E. T. 1983. ApJ 274, 152
- Vishniac E. T. 1994. ApJ 428, 186
- Williams, J. P., de Geus, E. J., & Blitz, L. 1994, ApJ, 428, 693
- Williams, J. P., Blitz, L. & Stark, A. 1995. ApJ 451, 252. (WBS95)
- Yonekura, Y., Dobashi, K., Mizuno, A., Ogawa, H., & Fukui, Y. 1997, ApJS 110, 21

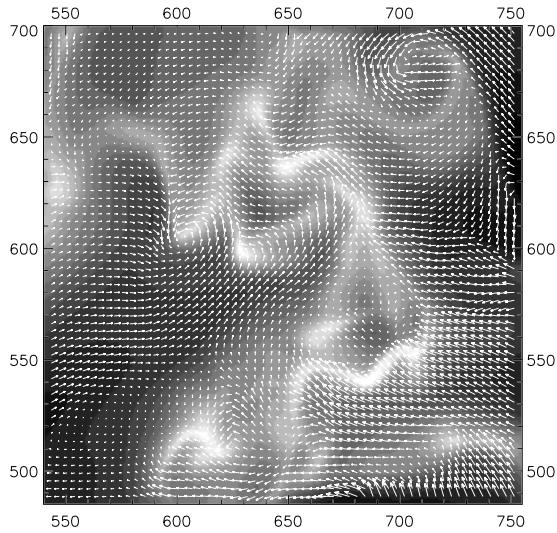
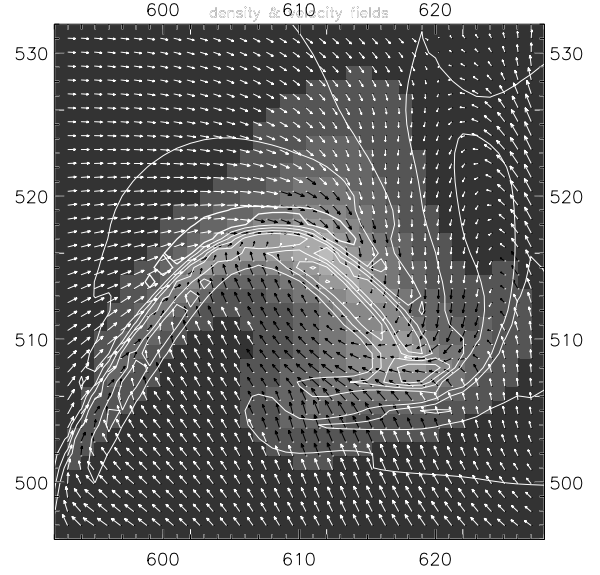
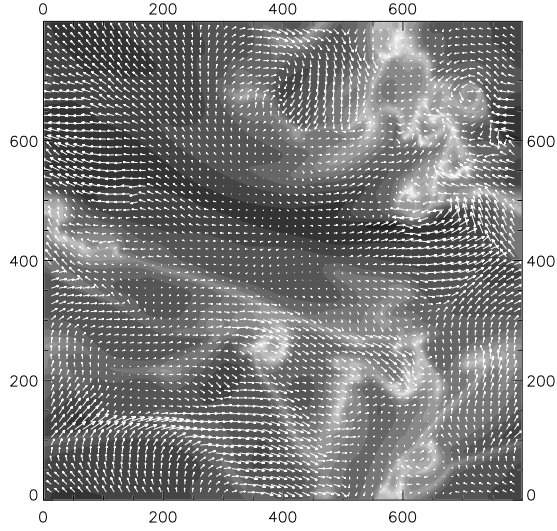


Fig. 1.— Three hierarchical levels of clouds in the simulation, showing the logarithmic density scale with shades of gray, and the velocity field with arrows. Pixel numbers are indicated by the grids. a) The whole simulation field, 800 pixels on a side, corresponding to 1 kpc. The gray scale shows structures with $\rho \geq \rho_T = 1.5 \text{ cm}^{-3}$ b) Magnification of the complex that appears when setting $\rho_T = 4$ in the upper right quadrant of fig. 1a. c) Magnification of the cloud that appears when setting $\rho_T = 8$ in the lower left region of fig. 1b. Black arrows indicate super-Alfvénic velocities in the frame moving with the cloud, and white arrows indicate sub-Alfvénic velocities. The contours give the magnetic field strength B . Thicker contours indicate larger B -values. The maximum density value is 55 cm^{-3} .

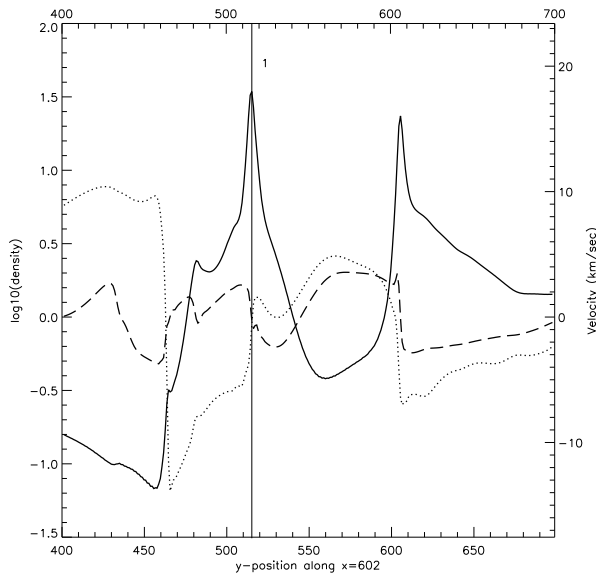
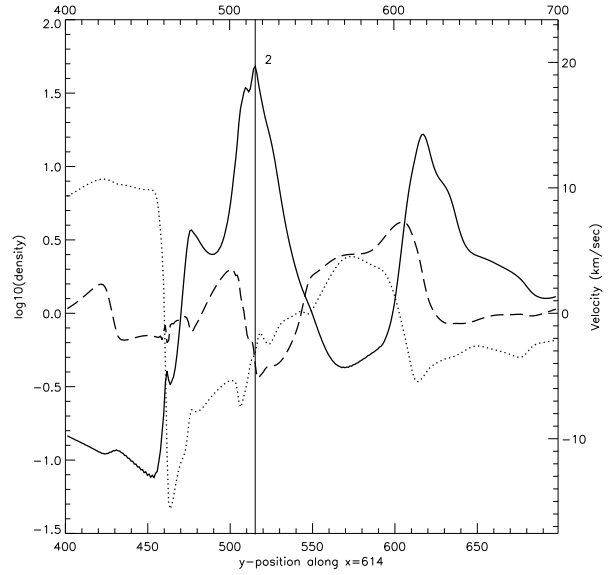
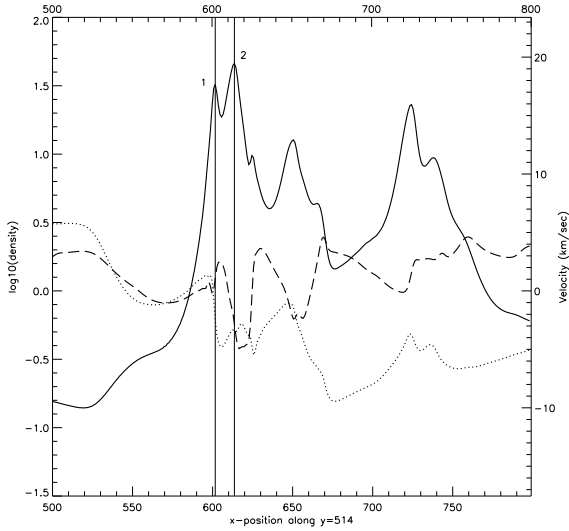


Fig. 2.— Cuts passing through the cloud shown in fig. 1c, (as indicated by the lines in fig. 3), showing the log of the density (solid line), and the x - (dotted line) and y - (dashed line) components of the velocity. a) Cut along x at $y = 514$. b) Cut along y at $x = 602$. c) Cut along y at $x = 614$. In a), two peaks are indicated. Peak 1 is seen to correspond to an x -shock (abrupt negative gradient) in a) and to a y -shock in b). Peak 2 is almost imperceptible in u_x , but is seen to correspond to a y -shock in c). Also, note the “plateau” in u_x extending 50 pixels to the right of peak 1, with average negative values, although with further substructure. Note that the scale is larger than in fig. 1c, in order to give a broader view of the velocity components.

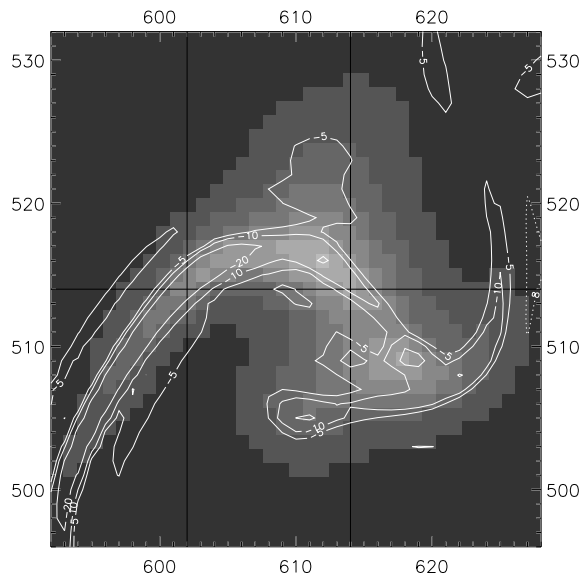


Fig. 3.— The same cloud as in fig. 1c, but with superimposed velocity divergence contours. Density maxima are seen to correspond to maximum negative values of the divergence. Also indicated are the lines along which the cuts of fig. 2 are taken.

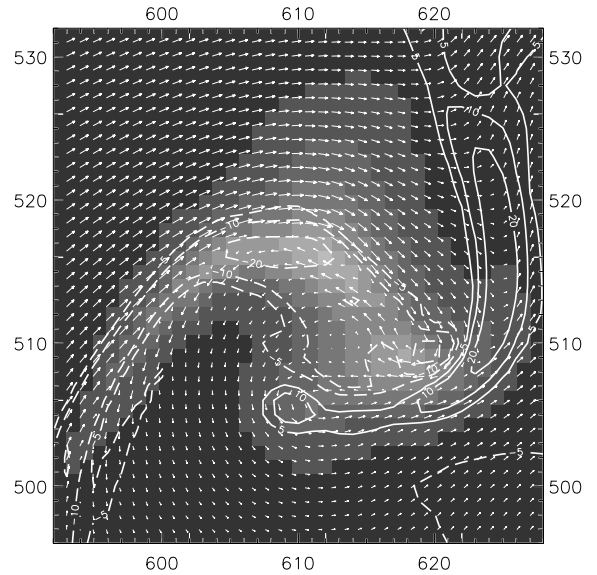


Fig. 4.— Same cloud as in fig. 1c, but with superimposed vorticity contours. There is a significant correlation between the density (and therefore the divergence) and the vorticity fields. We interpret this as a result of the generally oblique nature of the stream collisions. Solid (dashed) contours indicate positive (negative) vorticity. Also shown are the magnetic field vectors (arrows). Note the correlation between density and magnetic field bendings and the field reversal along the central ridge of the cloud. Note also the general alignment of the field with the density, although at many places the field crosses the cloud’s “boundary” perpendicularly (e.g., at the concave region below the left filament).

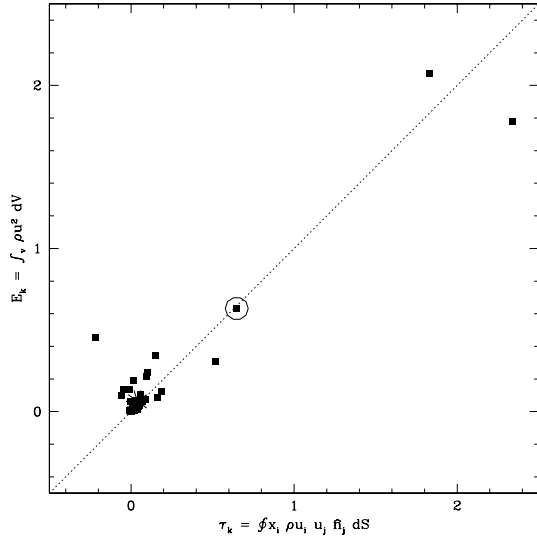


Fig. 5.— Kinetic energy \mathcal{E}_{kin} vs. the kinetic surface term τ_{kin} for all clouds with areas larger than 300 pixels in the whole field. The complex of fig. 1b is shown by a circle, and the cloud in fig. 1c is shown by the star. Note the similarity of the two terms for most of the clouds, indicating that both contribute in similar amounts to the clouds’ virial balance.

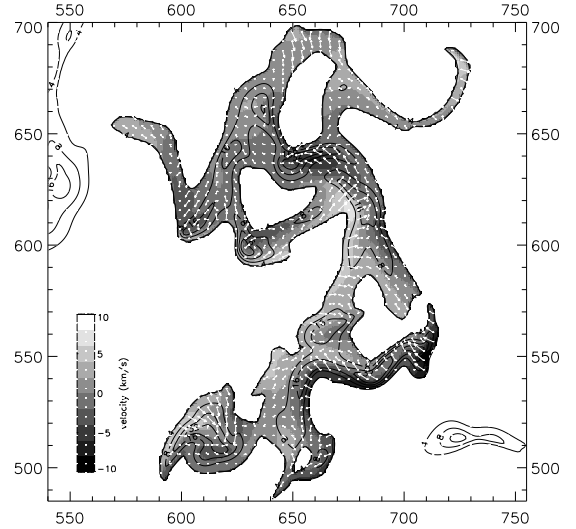


Fig. 7.— Same cloud as in fig. 1b, but indicating the magnitude of the local x -component of the velocity (gray-scale), in order to identify the origin of the x -velocity features appearing in the histogram of fig. 6. The velocity ranges are indicated in the sidebar. The arrows and contours indicate the velocity and the density fields, respectively. Three points are noticed. 1. The contribution to any given velocity interval originates from extended regions throughout the cloud. 2. Regions contributing to a given velocity interval contain zones of significantly different densities. 3. Regions with the same x -component of the velocity can have completely different total velocity vectors.

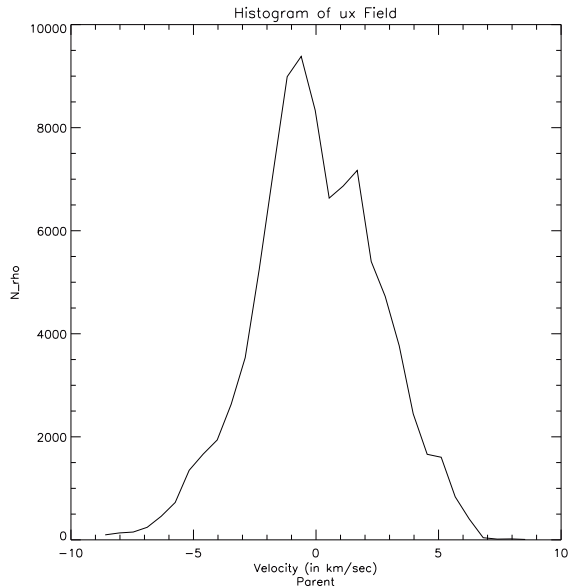


Fig. 6.— Density-weighted velocity histograms for the parent cloud (fig. 1b). Note the FWHM $\sim 5\text{--}7$ km s^{-1} , and the multi-component structure. Also, note the low-decaying wings.